



HAL
open science

FV-MHMM method for reservoir modeling

Jacques Franc, Laurent Jeannin, Gérald Debenest, Rolland Masson

► **To cite this version:**

Jacques Franc, Laurent Jeannin, Gérald Debenest, Rolland Masson. FV-MHMM method for reservoir modeling. Computational Geosciences, 2017, vol. 21 (n° 5/6), pp. 895-908. 10.1007/s10596-017-9644-1 . hal-01654666

HAL Id: hal-01654666

<https://hal.science/hal-01654666v1>

Submitted on 4 Dec 2017

HAL is a multi-disciplinary open access archive for the deposit and dissemination of scientific research documents, whether they are published or not. The documents may come from teaching and research institutions in France or abroad, or from public or private research centers.

L'archive ouverte pluridisciplinaire **HAL**, est destinée au dépôt et à la diffusion de documents scientifiques de niveau recherche, publiés ou non, émanant des établissements d'enseignement et de recherche français ou étrangers, des laboratoires publics ou privés.



Open Archive TOULOUSE Archive Ouverte (OATAO)

OATAO is an open access repository that collects the work of Toulouse researchers and makes it freely available over the web where possible.


This is an author-deposited version published in : <http://oatao.univ-toulouse.fr/>
Eprints ID : 18029

To link to this article : DOI:10.1007/s10596-017-9644-1
URL : <http://dx.doi.org/10.1007/s10596-017-9644-1>

To cite this version : Franc, Jacques and Jeannin, Laurent and Debenest, Gérald and Masson, Rolland [*FV-MHMM method for reservoir modeling*](#). (2017) Computational Geosciences, vol. 21 (n° 5/6). pp. 895-908. ISSN 1420-0597 Item availability restricted.

Any correspondence concerning this service should be sent to the repository administrator: staff-oatao@listes-diff.inp-toulouse.fr

FV-MHMM method for reservoir modeling

J. Franc¹  · L. Jeannin^{2,4} · G. Debenest¹ · R. Masson³

Abstract The present paper proposes a new family of multiscale finite volume methods. These methods usually deal with a dual mesh resolution, where the pressure field is solved on a coarse mesh, while the saturation fields, which may have discontinuities, are solved on a finer reservoir grid, on which petrophysical heterogeneities are defined. Unfortunately, the efficiency of dual mesh methods is strongly related to the definition of up-gridding and down-gridding steps, allowing defining accurately pressure and saturation fields on both fine and coarse meshes and the ability of the approach to be parallelized. In the new dual mesh formulation we developed, the pressure is solved on a coarse grid using a new hybrid formulation of the parabolic problem. This type of multiscale method for pressure equation called multiscale hybrid-mixed method (MHMM) has been recently proposed for finite elements and mixed-finite element approach (Harder et al. 2013). We extend here the MH-mixed method to a finite volume discretization, in order to deal with large multiphase reservoir models. The pressure solution is obtained by solving a hybrid form of the pressure problem on the coarse mesh, for which

unknowns are fluxes defined on the coarse mesh faces. Basis flux functions are defined through the resolution of a local finite volume problem, which accounts for local heterogeneity, whereas pressure continuity between cells is weakly imposed through flux basis functions, regarded as Lagrange multipliers. Such an approach is conservative both on the coarse and local scales and can be easily parallelized, which is an advantage compared to other existing finite volume multiscale approaches. It has also a high flexibility to refine the coarse discretization just by refinement of the lagrange multiplier space defined on the coarse faces without changing nor the coarse nor the fine meshes. This refinement can also be done adaptively w.r.t. a posteriori error estimators. The method is applied to single phase (well-testing) and multiphase flow in heterogeneous porous media.

Keywords Multiscale method · Finite volume method · Reservoir modeling

1 Introduction

Upscaling and scaling laws in science remain a challenge. Finding ways to deal with complex phenomena at a given scale and then, producing a mathematical model able to represent this physics, at the so-called macroscale, is difficult for many fields (hydrology, reservoir engineering, meteorology, etc...) [25].

For single-phase incompressible flows in porous media, pressure field obeys the following elliptic equation:

$$\begin{aligned} \nabla \cdot (-K(\mathbf{x})\nabla u) &= f \quad \text{in } \Omega, \\ u &= u_g \quad \text{on } \partial\Omega. \end{aligned} \quad (1)$$

where $K(\mathbf{x})$ is a symmetric and positive definite tensor defined at the Darcy's scale. The permeability distribution

✉ J. Franc
jacques.franc@imft.fr

¹ Institut de Mécanique des Fluides (IMFT) - Université de Toulouse, CNRS-INPT-UPS, 31400 Toulouse, France

² Storengy, Immeuble Djinn, 12 rue Raoul Nordling, 92274 Bois-Colombes, France

³ Laboratoire de Mathématiques J.A. Dieudonné, UMR 7351 CNRS, University Nice Sophia Antipolis, 06108 Nice, France

⁴ ENGIE E&P International, Faubourg de l'Arche, 1 place Samuel de Champlain, 92930 La Défense, France

in space yields correlated structures that span several orders of magnitude. The link between the local scale, that is the Darcy-scale where $K(\mathbf{x})$ is locally varying, to a larger scale such as the reservoir scale was and continues to be the object of much attention in order to predict accurate fluid flows in porous media. When the medium is homogeneous or large enough for length scales to be separated, the problem is well understood and references are easy to find (see for instance [21]). However, when there is no length scale separation or when two-phase flow problems are studied (i.e., when pressure field is coupled with a saturation field strongly dependent on local heterogeneity), details of the permeability at the Darcy-scale must be kept in order to correctly describe flow in porous media.

Numerous multiscale algorithms are available to address this problem. Unlike traditional methods, multiscale approaches benefit from keeping information on the underlying details. Examples of these methods can be found in multiscale finite element methods (MsFEM) [8, 15], numerical subgrid methods (NSub) [2] or the multiscale finite volume method (MsFv) [16, 17]. All these methods address the problem by embedding Darcy-scale informations from resolution of the sub-problems into the resolution of a reservoir-scale discretized problem. MsFEM [8, 15] detailed and improved in [1], relies on the construction of a local basis function suited to the heterogeneities. Local velocity, ensuring mass conservation, is obtained using a mixed formulation. NSub proposes a different approach based on the decomposition of pressure into a coarse scale pressure and its subscale variation on fine scale. Coarse scale pressure is approximated using RT₀ [20] or BDM₁ [3] spaces while subscale variations use RT₀ spaces on the fine scale. Eventually MsFv formulates a method that obtains pressure as a linear combination of constructed coarse scale basis functions that embed fine scale variations. MsFv has to construct a dual grid in order to build its global system. Applying boundary conditions can be tedious [10]. Moreover, it has been reported [24] that MsFv, without smoothing steps, can not solve some of the 10th SPE [9] slices as it only resolves low frequency errors. It will be highlighted in the numerical tests.

This paper intends to develop a new finite volume multiscale method (FV-MHMM) derived from the multiscale hybrid-mixed method (MHMM) formulated for finite elements and the mixed-finite element approach [12, 13]. The pressure equation is solved using a hybrid formulation on the coarse mesh, for which the unknowns are fluxes defined on the coarse mesh faces. Basis functions required for the construction of the coarse-scale system (referred to as the global system) are obtained by solving two kinds of local problems, which account for heterogeneities in the permeability field but also for the treatment of the local source terms (e.g., wellbore pressure). The pressure continuity

between coarse cells is then ensured by regarding flux basis functions as Lagrange multipliers. Such a method ensures mass conservation on both the local and global scales. It also offers the possibility of improving the coarse scale solution by refining the Lagrange multiplier space defined on coarse faces without changing either the coarse discretization or the fine mesh grid. This method offers the possibility of adaptive refinement with respect to a posteriori estimators.

The first section is dedicated to the mathematical formulation of the FV-MHMM method. The construction of the two kinds of local basis functions and the formulation of a global problem, including Lagrange multipliers as flux unknowns, are exposed. The second section presents selected numerical test cases. It is divided into three parts. The first part studies the convergence behavior of the method and gives the results on a heterogeneous permeability field. The second part presents the adaptation of the FV-MHMM method to slightly compressible flows and the third part extends this approach to two-phase flow, coupling the pressure equation with a fine scale updated equation of saturation.

2 Mathematical development

2.1 Multiscale hybrid-mixed method

Let us define a polyhedral (polygonal in 2D) coarse mesh of the domain Ω by its set M_H of coarse cells $K \in M_H$ and its set of coarse planar faces (edges in 2D) F_H . On each coarse face of F_H , we define the unit normal vector \mathbf{n} with a fixed orientation taking care to ensure that it is oriented outward on $\partial\Omega$. For each coarse cell $K \in M_H$, the unit normal vector on ∂K oriented outward to ∂K is denoted by \mathbf{n}_K .

The multiscale hybrid-mixed method developed in [12, 13] is based on the following primal hybrid variational formulation of Eq. 1 introduced in [20] which weakly enforces the continuity of the solution at the coarse faces F_H through the action of Lagrange multipliers:

$$\begin{aligned} & \text{find } (u, \lambda) \in V \times \Lambda \text{ such that:} \\ & \int_{\Omega} K(\mathbf{x}) \nabla u \cdot \nabla v dx + \sum_{K \in M_H} \int_{\partial K} \lambda \mathbf{n} \cdot \mathbf{n}_K v|_K d\sigma \\ & \quad + \sum_{K \in M_H} \int_{\partial K} \mu \mathbf{n} \cdot \mathbf{n}_K u|_K d\sigma = \int_{\Omega} f v dx \\ & \quad + \int_{\partial\Omega} \mu u_g d\sigma \quad \text{for all } (v, \mu) \in V \times \Lambda. \end{aligned} \tag{2}$$

where V is the broken Sobolev space $H^1(M_H)$ defined by

$$H^1(M_H) = \{v \in L_2(\Omega) : v|_K \in H^1(K), K \in M_H\},$$

Λ stands for the following Lagrange multipliers space

$$\Lambda := \left\{ \mu \in \prod_{K \in M_H} H^{-\frac{1}{2}}(\partial K) : \exists \sigma \in \times H_{div}(\Omega) \text{ s.t. } \mu|_{\partial K} = \sigma \cdot \mathbf{n}|_{\partial K}, K \in M_H \right\},$$

∇v is the broken gradient equal to $\nabla v|_K$ on each coarse cell $K \in M_H$, $H_{div}(\Omega)$ is defined as:

$$H_{div}(\Omega) := \{ \sigma \in [L^2(\Omega)]^d : \nabla \cdot \sigma \in L^2(\Omega) \},$$

and $H^{-\frac{1}{2}}(\partial K)$ is the dual space of the space $H^{\frac{1}{2}}(\partial K)$ span by the traces on ∂K of functions in $H^1(K)$.

Let us denote by V_0 the space of cellwise constant functions in each coarse cell $K \in M_H$ and by W_K the set of functions in $H^1(K)$ with zero mean value on K . Then, $W := \prod_{K \in M_H} W_K$ is a subspace of V such that we have the orthogonal decomposition

$$V = V_0 \oplus W = V_0 \oplus \bigoplus_{K \in M_H} W_K.$$

Following this decomposition, each $v \in V$ is uniquely decomposed as $v = v_{0,K} + \sum_{K \in M_H} \tilde{v}_K$ with $v_{0,K} \in V_0$ and $\tilde{v}_K \in W_K$ which leads to the splitting of the previous variational formulation as the sum of two local problems set on W_K for each coarse cell $K \in M_H$ and a global problem set on $V_0 \times \Lambda$.

For a given $\lambda \in \Lambda$, the first local problem, referred to as the local lambda problem (LLP) in the following, writes (see [12, 13] for details): Find $\tilde{u}_K \in W_K$ such that:

$$\int_K K(\mathbf{x}) \nabla \tilde{u}_K \cdot \nabla \tilde{v}_K dx + \int_{\partial K} \lambda \mathbf{n} \cdot \mathbf{n}_K \tilde{v}_K d\sigma = 0 \quad \text{for all } \tilde{v}_K \in W_K, \quad (3)$$

and we set $\tilde{u}_K = T_K \lambda$.

The second local problem dealing with the source term f and referred to as the local source problem (LSP) in the following, writes (see [12, 13] for details): Find $\tilde{u}_K \in W_K$ such that:

$$\int_K K(\mathbf{x}) \nabla \tilde{u}_K \cdot \nabla \tilde{v}_K dx = \int_K f \tilde{v}_K dx \quad \text{for all } \tilde{v}_K \in W_K, \quad (4)$$

and we set $\tilde{u}_K = \hat{T}_K f$.

The global problem solve the coarse conservation equations together with the trace continuity equations at the coarse interfaces (see [12, 13] for a detailed analysis of this formulation): find $u_{0,K} \in \mathbb{R}$, $K \in M_H$ and $\lambda \in \Lambda$ such that:

$$\left\{ \begin{array}{l} \sum_{K \in M_H} \int_{\partial K} \lambda \mathbf{n} \cdot \mathbf{n}_K d\sigma = \int_K f dx \quad \text{for all } K \in M_H, \\ \sum_{K \in M_H} \int_{\partial K} \mu \mathbf{n} \cdot \mathbf{n}_K (u_{0,K} + T_K \lambda + \hat{T}_K f) d\sigma \\ = \int_{\partial \Omega} \mu u_g \quad \text{for all } \mu \in \Lambda. \end{array} \right. \quad (5)$$

The objective of the next subsection is to specify the MHM method when a Two Point Flux finite volume scheme is used to solve the local problems.

2.2 MHM method coupled with a two point flux approximation (TPFA) of the local problems

Each coarse cell K is submeshed with an orthogonal fine mesh and we denote by $M_{h,K}$ the set of sub-cells, by $F_{h,K}^{int}$ the set of interior faces and by $F_{h,K}^{ext}$ the set of boundary faces. The set of faces of the cell $X \in M_{h,K}$ is denoted by $F_X \subset F_{h,K}^{int} \cup F_{h,K}^{ext}$. The set of two cells sharing the interior face $\sigma \in F_{h,K}^{int}$ is denoted by $M_\sigma = \{X, Y\}$ and the notation $X|Y$ will also be used to denote the face σ at the interface between the two cells.

Let $V_{h,K}$ be the space of cellwise constant functions in each cell $X \in M_{h,K}$. For $u_{h,K} \in V_{h,K}$, we denote by u_X the value of $u_{h,K}$ in the cell X for all $X \in M_{h,K}$. V_h will denote the space of cell-wise constant functions on each cell $X \in M_h = \bigcup_{K \in M_H} M_{h,K}$ and for $u_h \in V_h$, $u_{h,K}$ denotes the restriction of u_h to the coarse cell K . Let us set

$$W_{h,K} = \{ u_{h,K} \in V_{h,K} \mid \sum_{X \in M_{h,K}} |X| u_X = \int_K u_{h,K}(x) dx = 0 \}.$$

Let us denote by $V_{h,\partial K} \subset L^2(\partial K)$ the set of piecewise constant functions on each face $\sigma \in F_{h,K}^{ext}$. For $u_{h,\partial K} \in V_{h,\partial K}$, we denote by $u_{K,\sigma}$ the value of $u_{h,\partial K}$ on the face $\sigma \in F_{h,K}^{ext}$. The approximate solution in each coarse cell K and the approximate trace on ∂K , $K \in M_H$ will be denoted by $(u_{h,K}, u_{h,\partial K}) \in V_{h,K} \times V_{h,\partial K}$.

Let $(v_{h,K}, v_{h,\partial K}) \in V_{h,K} \times V_{h,\partial K}$, the two point flux approximation (TPFA) at the face $\sigma \in F_X \cap F_{h,K}^{int}$ outward to the cell X is defined by

$$F_{X,Y}(v_X, v_Y) = F_{X,\sigma}(v_X, v_Y) = T_\sigma(v_X - v_Y), \quad M_\sigma = \{X, Y\},$$

where T_σ is the transmissivity of the interior face σ , and the TPFA at the boundary face $\sigma \in F_X \cap F_{h,K}^{ext}$ outward to the cell X is given by

$$F_{X,\sigma}(v_X, v_{K,\sigma}) = T_{X,\sigma}(v_X - v_{K,\sigma}),$$

where $T_{X,\sigma}$ is the half transmissivity of the boundary face σ .

Let Λ_H denote a finite dimensional subspace of $L^2(F_H)$.

2.2.1 Local problems

Using the finite volume scheme with TPFA, the discretization of the *LLP* local problem (3) is given by the following discrete variational formulation: given $\lambda \in \Lambda_H$,

find $(u_{h,K}, u_{h,\partial K}) \in W_{h,K} \times V_{h,\partial K}$ such that for all $(v_{h,K}, v_{h,\partial K}) \in W_{h,K} \times V_{h,\partial K}$ one has

$$\left\{ \begin{array}{l} \sum_{\sigma \in X|Y \in F_{h,K}^{int}} T_{\sigma}(u_X - u_Y)(v_X - v_Y) \\ + \sum_{\sigma \in F_{h,K}^{ext}, \sigma \in F_X} T_{X,\sigma}(u_X - u_{K,\sigma})(v_X - v_{K,\sigma}) \\ + \sum_{\sigma \in F_{h,K}^{ext}} \int_{\sigma} v_{K,\sigma} \lambda \mathbf{n} \cdot \mathbf{n}_K d\sigma = 0. \end{array} \right.$$

Using a Lagrange multiplier to deal with the zero mean value constraint for the test functions in $W_{h,K}$, it is easy to show that this discrete variational formulation is equivalent to the following finite volume conservation equations: find $(u_{h,K}, u_{h,\partial K}) \in W_{h,K} \times V_{h,\partial K}$ such that

$$\begin{aligned} \sum_{\sigma \in X|Y \in F_X \cap F_{h,K}^{int}} T_{\sigma}(u_X - u_Y) + \int_{\partial K \cap \partial X} \lambda \mathbf{n} \cdot \mathbf{n}_K d\sigma \\ = \frac{|X|}{|K|} \int_{\partial K} \lambda \mathbf{n} \cdot \mathbf{n}_K d\sigma, \end{aligned}$$

for all $X \in M_{h,K}$, and

$$F_{X,\sigma}(u_X, u_{K,\sigma}) = T_{X,\sigma}(u_X - u_{K,\sigma}) = \int_{\sigma} \lambda \mathbf{n} \cdot \mathbf{n}_K d\sigma,$$

at each face $\sigma \in F_{h,K}^{ext} \cap F_X$. Let us define the operators $(T_{h,K}, T_{h,\partial K})$ mapping Λ_H to $L^2(K) \times L^2(\partial K)$ and such that $(T_{h,K}\lambda, T_{h,\partial K}\lambda)$ is equal to the solution $(u_{h,K}, u_{h,\partial K})$ of the previous local problem.

Similarly, the functions $(\hat{T}_{h,K}f, \hat{T}_{h,\partial K}f)$ are defined for $f \in L^2(\Omega)$ by the solution $(u_{h,K}, u_{h,\partial K}) \in W_{h,K} \times V_{h,\partial K}$ of the finite volume conservation equations discretizing the LSP local problem (4):

$$\sum_{\sigma \in X|Y \in F_X \cap F_{h,K}^{int}} T_{\sigma}(u_X - u_Y) = \int_X f dx - \frac{|X|}{|K|} \int_K f dx,$$

for all $X \in M_{h,K}$, and $u_{K,\sigma} = u_X$ for all $\sigma \in F_{h,K}^{ext} \cap F_X$. Let us remark that we have for all $(\lambda, \mu) \in \Lambda_H \times \Lambda_H$

$$\left\{ \begin{array}{l} \int_{\partial K} \mu \mathbf{n} \cdot \mathbf{n}_K T_{h,\partial K} \lambda d\sigma = \int_{\partial K} \lambda \mathbf{n} \cdot \mathbf{n}_K T_{h,\partial K} \mu d\sigma \\ = - \sum_{\sigma \in X|Y \in F_{h,K}^{int}} T_{\sigma}(u_X - u_Y)(v_X - v_Y) \\ - \sum_{\sigma \in F_{h,K}^{ext}, \sigma \in F_X} T_{X,\sigma}(u_X - u_{K,\sigma})(v_X - v_{K,\sigma}), \end{array} \right.$$

with $(u_{h,K}, u_{h,\partial K}) = (T_{h,K}\lambda, T_{h,\partial K}\lambda)$, $(v_{h,K}, v_{h,\partial K}) = (T_{h,K}\mu, T_{h,\partial K}\mu)$ which implies that the bilinear form

$$a_{h,K}(\lambda, \mu) = - \int_{\partial K} \mu \mathbf{n} \cdot \mathbf{n}_K T_{h,\partial K} \lambda d\sigma,$$

on $\Lambda_H \times \Lambda_H$ is symmetric positive. The bilinear form $a_{h,K}$ is also definite if the restriction of the space Λ_H to ∂K is not ‘‘finer’’ than the space of piecewise constant functions on the fine faces of ∂K .

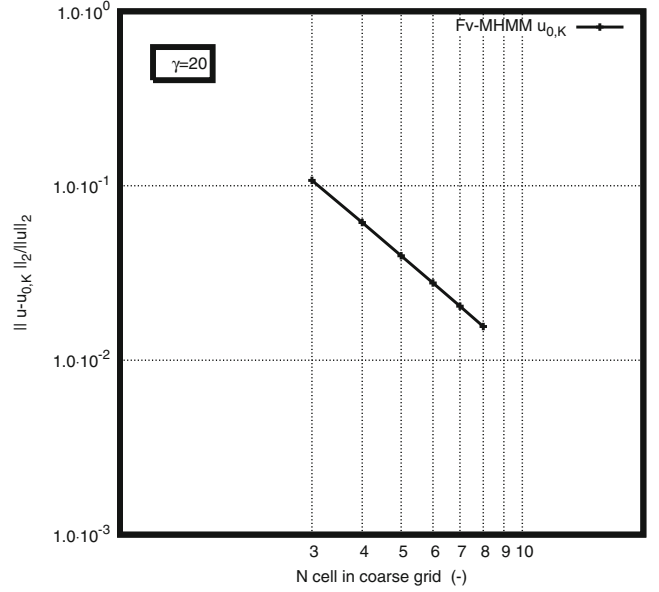


Fig. 1 Convergence behavior of $u_{0,K}$ with respect to coarse grid refinement for homogeneous permeability field

2.2.2 Global problem

The discrete global problem is just obtained by replacing in (5) the vector space Λ by the discrete vector space Λ_H and the trace on ∂K of the continuous operators T_K and \hat{T}_K by respectively the operators $T_{h,\partial K}$ and $\hat{T}_{h,\partial K}$ leading to the following set of discrete equations:

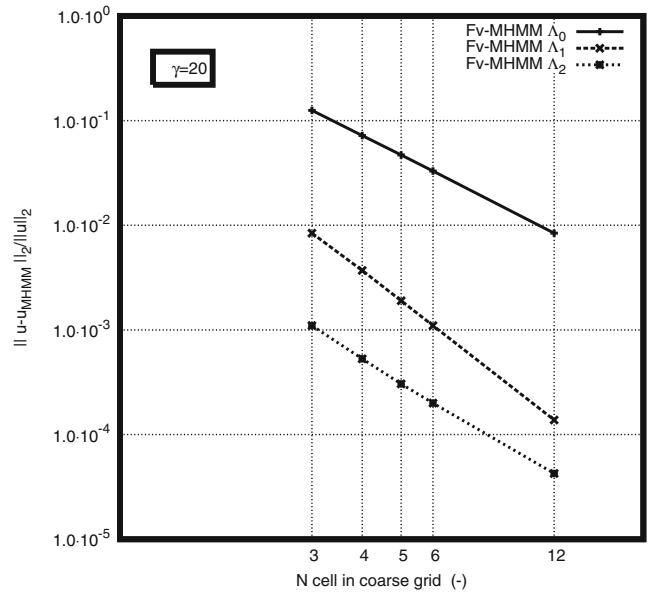


Fig. 2 Convergence for different Λ_l space on a homogeneous Laplacian case

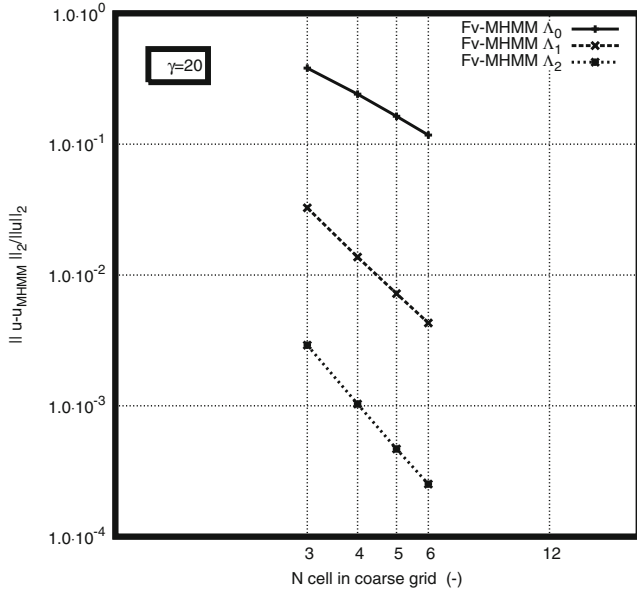
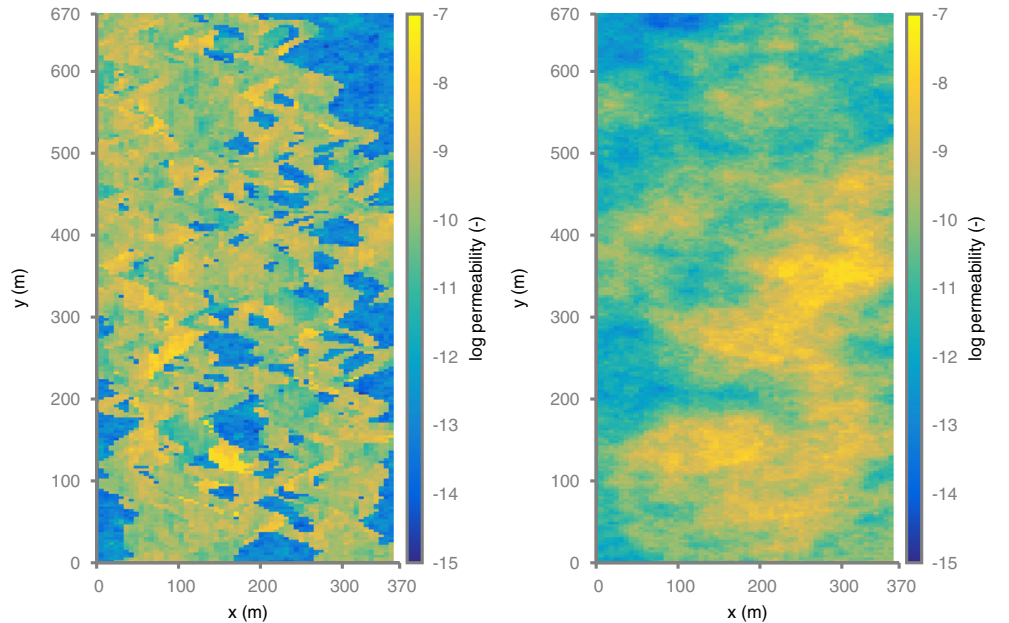


Fig. 3 Convergence for different Λ_l space with sinusoidal source term

find $u_{0,K} \in \mathbb{R}$, $K \in M_H$ and $\lambda \in \Lambda_H$ such that:

$$\begin{cases} \sum_{K \in M_H} \int_{\partial K} \lambda \mathbf{n} \cdot \mathbf{n}_K d\sigma = \int_K f dx & \text{for all } K \in M_H, \\ \sum_{K \in M_H} \int_{\partial K} \mu \mathbf{n} \cdot \mathbf{n}_K (T_{h,\partial K} \lambda + u_{0,K}) d\sigma = \int_{\partial \Omega} \mu u_g d\sigma \\ - \sum_{K \in M_H} \int_{\partial K} \mu \mathbf{n} \cdot \mathbf{n}_K \hat{T}_{h,\partial K} f d\sigma & \text{for all } \mu \in \Lambda_H. \end{cases}$$

Fig. 4 Map of log permeability of a fluvial and near-shore typed slices of the 10th SPE case



The first equation is a direct transcription of coarse scale mass conservation while the second equation weakly enforces the trace continuity at coarse interfaces.

Roughly speaking, this mixed linear system (or saddle point problem) will be non singular if Λ_H contains, for each coarse face $\sigma \in F_H$, at least one function supported on σ with non zero mean value on σ , and if Λ_H is not *finer* than the space of piece-wise constant functions on the fine faces of F_H .

In the following 2D numerical test cases, the vector space Λ_H will be typically defined as the vector space of polynomials of degree l on each coarse face of F_H with $l = 0, 1, 2$. These choices of Λ_H will be denoted by Λ_l , $l = 0, 1, 2$ in the following.

Given a basis of Λ_H denoted by $\lambda_{\sigma,i}$ for all $\sigma \in F_H$, $i = 1, \dots, n_\sigma$, the assembly of the global matrix can be done by computing on each coarse cell K the symmetric negative local rigidity matrix defined by

$$(A_K)_{\sigma_1, i_1}^{\sigma_2, i_2} = \int_{\partial K} \lambda_{\sigma_1, i_1} \mathbf{n} \cdot \mathbf{n}_K T_{h,\partial K} \lambda_{\sigma_2, i_2} d\sigma, \quad (7)$$

with $\sigma_1, \sigma_2 \in F_{h,K}$, $i_1 = 1, \dots, n_{\sigma_1}$, $i_2 = 1, \dots, n_{\sigma_2}$, as well as the local vector defined by

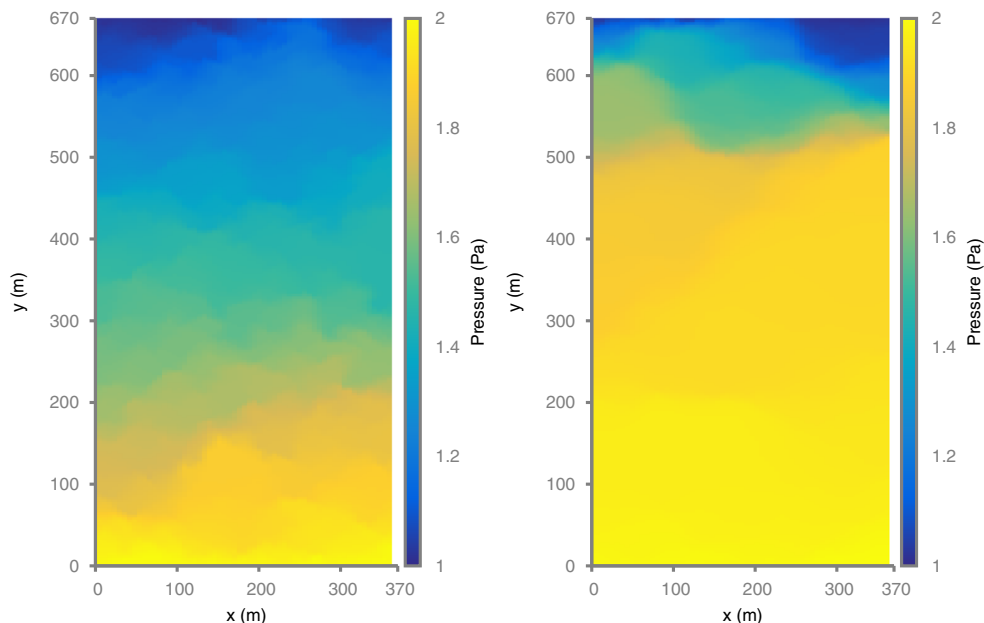
$$(B_K)_{\sigma, i} = \int_{\partial K} \lambda_{\sigma, i} \mathbf{n} \cdot \mathbf{n}_K \hat{T}_{h,\partial K} f d\sigma, \quad \sigma \in F_{h,K}, i = 1, \dots, n_\sigma. \quad (8)$$

and doing the global assembly in the finite element fashion.

In order to assess the amount of CPU workloads at each time step, a complexity analysis similar to the analysis of

(6)

Fig. 5 Finite volume reference solutions of a fluvial and near-shore typed slices of the 10th SPE case



[16] is reported in Appendix A. The time spent in the global stage is indeed larger than in the *MsFv* method, but the overall process is found to be faster for constant ($l = 0$) or linear ($l = 1$) basis and as fast for quadratic ($l = 2$).

3 Numerical tests

In this section, numerical tests on different formulations of the FV-MHMM algorithm are performed. In the first subsection, convergence and heterogeneous test cases for incompressible formulation are presented. The second subsection shows how to adapt the algorithm to slightly compressible flows and presents a basic example of a production wellbore in a bounded reservoir. In the last subsection, a two-phase case permits to present the adaptation of the method to multiphase flow and allows comparisons with well-known Buckley-Leverret solution.

3.1 Incompressible algorithm

Incompressible formulation of the method is now tested in various configurations. Firstly, the convergence characteristic behavior of the method is assessed for two simple cases. The convergence study on the piecewise constant coarse cell unknown $u_{0,K}$ is reported to be h^2 -convergent independently of case treated or Λ_l considered. The analysis for a homogeneous permeability field is chosen (see on Fig. 1). The independence of $u_{0,K}$ convergence rate to the polynomial functions' subspace Λ_l chosen is also denoted in [12].

3.1.1 Convergence on a homogeneous permeability field

Simulations are performed solving Eq. 1 with an isotropic permeability field, reducing the tensor $K(\mathbf{x})$ to the scalar parameter $K = 1$. For the first test, the source term value is $f(x, y) = 1$ throughout the whole square domain of extend $a = 1$. On the boundaries of the global domain, unknown is weakly imposed to $u_g = 0$. Meshgrids are uniformly discretized with the same number of cells along each direction. Let us then define γ as the number of fine cells embedded in a coarse cell along one direction. Convergence study is performed keeping γ constant (see on Fig. 2).

The error is measured as L_2 -norm of the relative error between reconstructed field $u_h = u_{0,K} + \tilde{u}_\lambda + \tilde{u}_f$ to a semi-analytical solution taken from [6]. The solution is expressed as an infinite sum which is truncated for the study at $n = 200$:

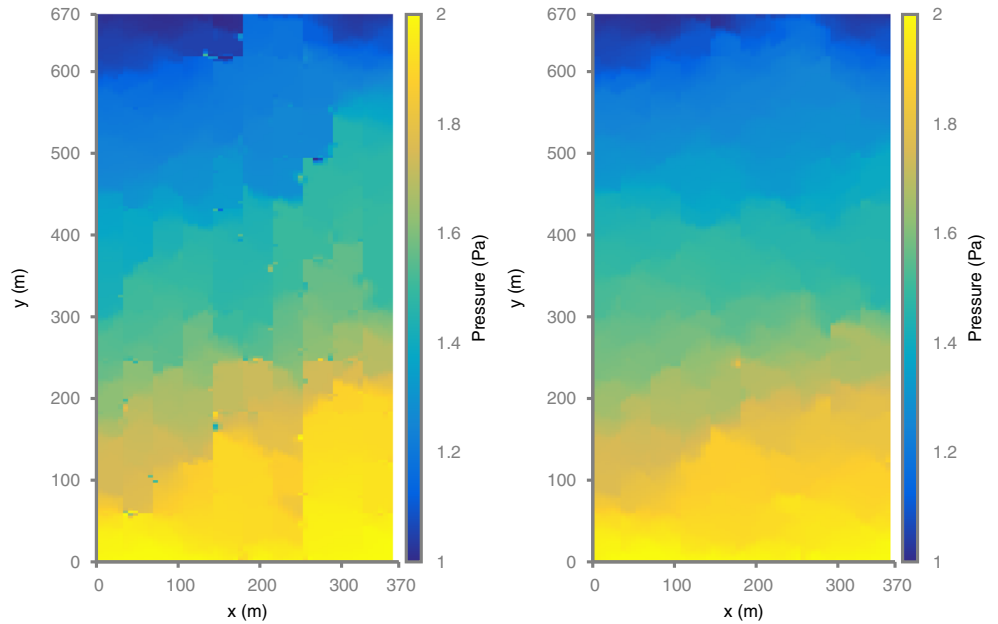
$$u(x, y) = \frac{(a^2 - x^2)}{2} - \frac{16a^2}{\pi^3} \sum_{n=0}^{\infty} \frac{(-1)^n \cos((2n+1)\pi x/2a) \cosh((2n+1)\pi y/2a)}{(2n+1)^3 \cosh((2n+1)\pi/2)}. \quad (9)$$

Convergence rate with respect to the coarse grid discretization depends on the Λ_l space chosen. Refining Λ_l

Table 1 Relative norm- L_2 error level refining Λ_l for a channelized SPE

	Basic	Transmissivity-weighted
Λ_1	0.033	0.0063
Λ_2	0.022	0.0047

Fig. 6 Result of incompressible single phase flow with basic and transmissivity weighted basis functions for Λ_1 on SPE slice with channelized medium (*i.e.* fluvial typed)



space ensures lower error levels for the same coarse grid discretization as reported in [12] (see on Fig. 2).

3.1.2 Convergence including sinusoidal source term

For the second test, the same problem as the previous case is performed, but including spatially varying source term. We impose the unknown to be null on the boundaries and the source term is modeled as a sinusoidal term following:

$$f(x, y) = 8\pi^2 \sin(2\pi x) \sin(2\pi y) \quad (10)$$

Same remarks as previously can be drawn from Fig. 3. The convergence behavior obtained for u_h is h^{l+2} -convergence on $\Lambda_l, l \in \{0, 1, 2\}$. This is comparable to the results of [12].

3.1.3 Study of heterogeneous sample

The next example is based on the 83th and the 13th slices proposed in the 10th SPE comparative solution project [9]. The former is a highly contrasted channelized permeability field typical of fluvial media, while the latter is heterogeneous typical of prograding near-shore environment. The domain is $370 \times 670 \text{ m}^2$. It is gridded using

Table 2 Relative norm- L_2 error level refining Λ_l for a near-shore typed SPE slice

	Basic	Transmissivity-weighted
Λ_1	0.0031	0.0010
Λ_2	0.0017	$5.9 \cdot 10^{-4}$

uniform Cartesian cells (60×220) as prescribed by the data set values for permeability. It is characterized respectively by a mean permeability value of $\mu(K) = 5.38 \cdot 10^{-10} \text{ m}^2$ and highly variable permeability background of variance $\sigma(\ln(K)) = 12.17$ for the channelized medium. The 13th slice is characterized by a mean permeability value of $\mu(K) = 6.07 \cdot 10^{-10} \text{ m}^2$ and mildly variable permeability background of variance $\sigma(\ln(K)) = 6.01$. Their logarithmic map are shown on Fig. 4. We impose a constant pressure drop, $\Delta u = 1 \text{ Pa}$, between opposite faces in the y -direction. A no-flux condition is imposed on the other boundaries. A reference finite volume solution is obtained on the fine grid and reported on Fig. 5. Software used is an OpenFOAM developed code [14]. Performances of $\Lambda_l, l \in \{1, 2\}$ spaces are evaluated on a coarse grid of 10×11 cells.

Let us consider first the case of a channelized permeability. As expected, increasing the order of polynomial space Λ_l allows us to capture more details of the channelized flow. However, the L_2 -norm error level for Λ_2 remains high as reported on Table 1.

It is then important to optimize the choice of test functions used in the local problems (LLP and LSP). To this effect, a fine scale transmissivity weighted method can be used in the local LLP and global problems construction in

Table 3 Means and standard deviation of L_2 -norm error w.r.t the type of heterogeneities

	Tarbert facies	Upper-Ness facies
MsFv	0.03(0.017)	0.438(0.589)
FV-MHMM- $\Lambda_2(\text{reg})$	$2.61(0.41) \cdot 10^{-3}$	0.072(0.029)
FV-MHMM- $\Lambda_2(\text{tw})$	$1.57(0.31) \cdot 10^{-3}$	0.011(0.007)

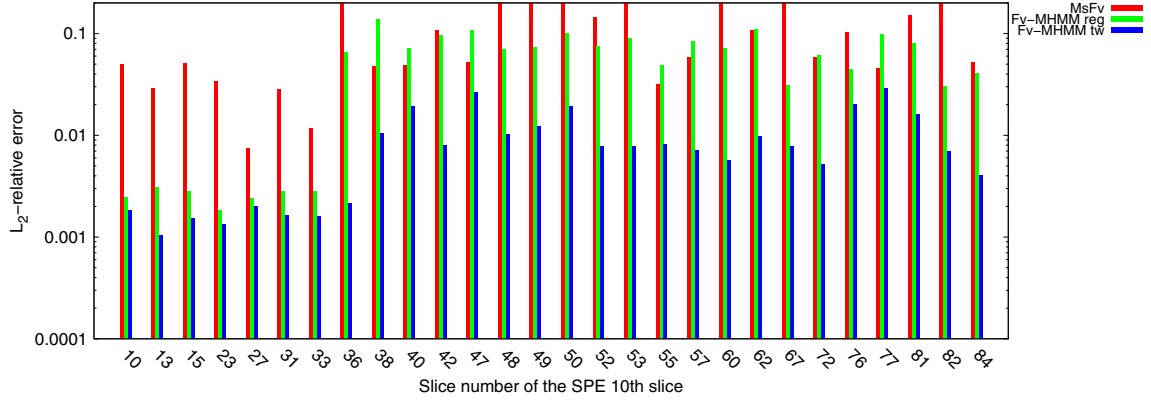


Fig. 7 L_2 relative errors of the pressure fields while solving incompressible single phase flow using MsFv, basic weighted and transmissivity weighted basis functions for Λ_1 on several of the SPE slices

the spirit of [23]. This consists in weighting the basis functions of the space Λ_l at each coarse face according to the fine faces transmissivities leading to a weighted choice of the Lagrange multiplier space Λ_H .

To be more specific, let us denote by $\sigma \in F_H$ a given coarse face. Let $F_{h,\sigma}$ denote the set of fine faces of the coarse face σ and T_e denote the transmissivity of the fine face e . The new basis functions of Λ_H are defined on each coarse face σ by

$$\lambda_{\sigma,i}(s) = s^i \frac{T_e}{\sum_{e \in F_{h,\sigma}} T_e}, i = 0, \dots, l,$$

where l is the polynomial degree of the space and s the coordinate along the 1D face σ . This choice of the

basis functions emphasizes high permeability areas over low permeability areas. It eases the flow to follow channel paths.

From Table 1, readers can observe that including a weighting scheme improves strongly the scheme convergence compared to unweighted basic approach. Indeed, the weighted scheme avoids trapping fluids in regions of low permeability and does not show the numerical artefacts present in the unweighted basic approach. The L_2 -norm error is then reduced more than 10 times using transmissivity-based weights.

As an example, we plot on Fig. 6 the pressure fields on the slice 73 comparing the basic and weighted schemes. This illustrates the ability of the modified model to treat the local heterogeneities related to high variations of the permeability fields. Consequently, when dealing with highly contrasted heterogeneous media, it is required to use the corrected FV-MHMM rather than the basic scheme.

Concerning the near-shore typed medium, FV-MHMM is efficient in its original formulation and errors between the two formulations of the same magnitude as reported in Table 2.

To conclude this section on heterogeneous fields, simulations has been performed on several of the 10th SPE heterogeneous slices comparing FV-MHMM with MsFv algorithm as it is implemented in MRST2016a [18]. MsFv is here considered as a stand-alone multiscale solver and no iterations are used in the reported results. Relative L_2 -norm errors with respect to the fine scale finite volume solution for the Λ_1 space are plotted on Fig. 7. The two main remarks developed above are highlighted in that graph. In representation of prograding near-shore porous medium (slice from number 1 to number 35), basic and weighted schemes for deriving local basis functions produce errors of the same order of magnitude. However, if a channelized medium

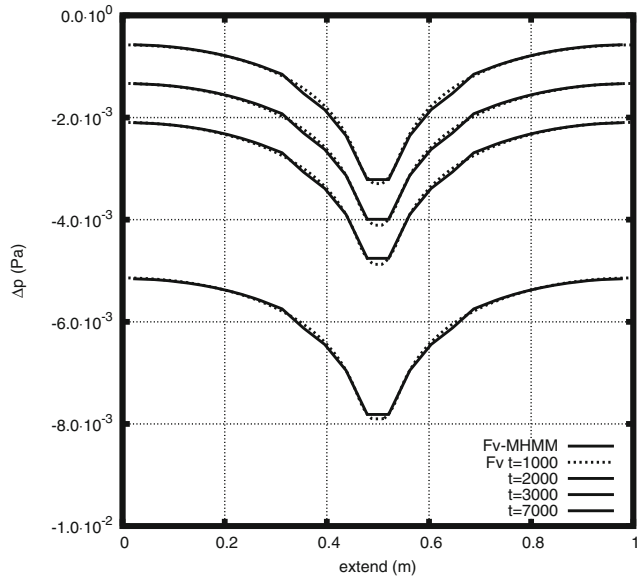


Fig. 8 Comparison between finite volume and FV-MHMM on injection case

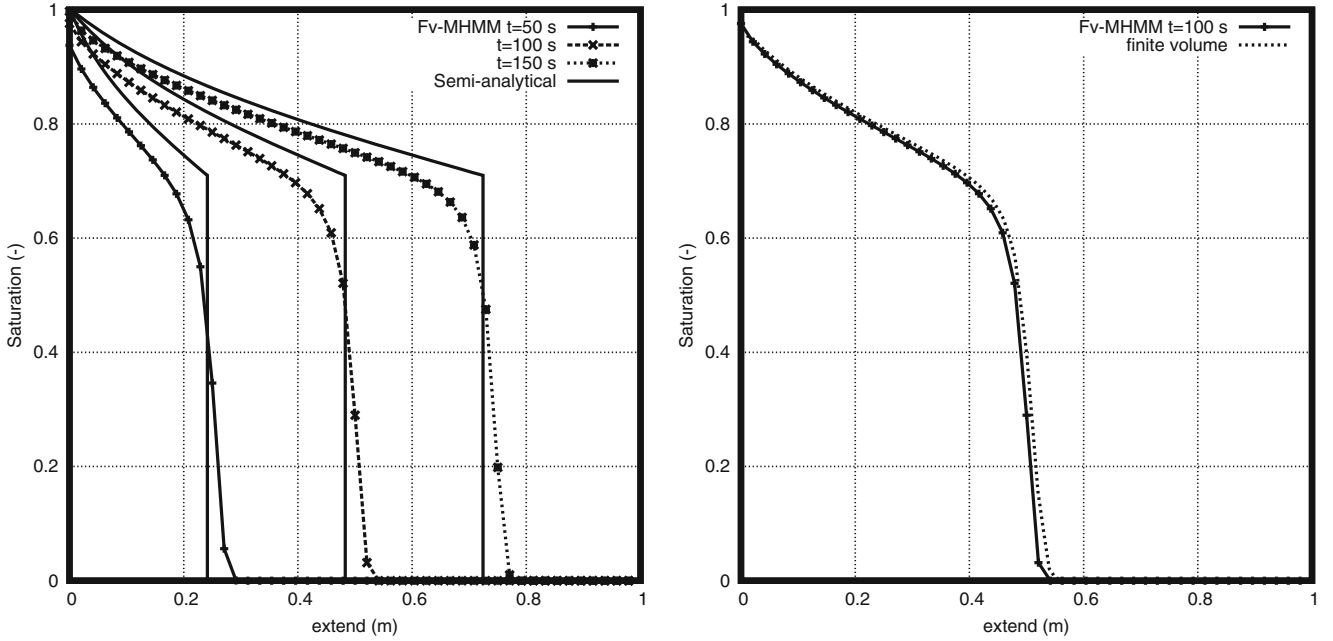


Fig. 9 Compared Buckley-Leverett: on the *left*, saturation front from semi-analytical and *FV-MHMM*; on the *right*, finite volume solutions and two-phase *FV-MHMM*

is considered, typical of fluvial environment (slice from number 36 to number 85), transmissivity weighted scheme improves significantly the accuracy. MsFv error reported on Fig. 7 are truncated as the method struggles to find a solution on some slices. As a comparable situation, the reader can refer to [24].

For the sake of completeness, Table 3 reports the mean value (and standard deviation) of the errors, considering slices by facies as if they were several equivalent realizations of an heterogeneous permeability field. On the Tarbert facies, weighted and unweighted formulations produce error of the same order of magnitude, but ten times smaller than MsFv. They also produce less discrepancy between the slices. The difficulties for MsFv to find a solution on some of the Upper-Ness facies are highlighted by a higher standard deviation values.

However, the latest development in the MsFv method proposed an algebraic version of the algorithm [7]. The method is then considered as a parallelizable preconditioner to a fine grid solver such as GMRES [19]. With this algebraic approach, convergence is reached on all of the 10th SPE slices.

3.2 Slightly compressible algorithm

The *FV-MHMM* method can be adapted to slightly compressible flows [13]. Introducing a compressibility parameter c such as $\frac{d\rho}{\rho} = c du$, the porosity ϕ and the viscosity μ ,

the elliptic system of (1) turns into the following parabolic equation:

$$\begin{aligned} \nabla \cdot \left(\frac{-K(\mathbf{x})}{\mu} \nabla u(\mathbf{x}, t) \right) + \phi c \frac{\partial u(\mathbf{x}, t)}{\partial t} &= f(\mathbf{x}, t) \quad \forall (\mathbf{x}, t) \in \Omega \times \mathbb{R}^+, \quad (11) \\ \frac{-K(\mathbf{x})}{\mu} \nabla u \cdot \mathbf{n} &= 0 \quad \forall (\mathbf{x}, t) \in \partial\Omega \times \mathbb{R}^+, \\ u(\mathbf{x}, 0) &= 0 \quad \forall \mathbf{x} \in \Omega. \end{aligned}$$

Following [13], the *FV-MHMM* algorithm can be adapted to solve such a parabolic problem based on the new orthogonal decomposition of the space V :

$$V = \bigoplus_{K \in M_H} V_K$$

with $V_K = H^1(K)$.

The local Lambda problem and local source problem can be rewritten in each coarse cell $K \in M_H$ after an Euler implicit time discretization (with time step Δt) and the TPGA discretization in space as follows:

$$\left\{ \begin{aligned} &\sum_{\sigma=X|Y \in F_X \cap F_{h,K}^{int}} T_\sigma (u_X - u_Y) + \int_X \phi c / \Delta t u_X dx \\ &+ \int_{\partial K \cap \partial \Omega} \lambda \mathbf{n} \cdot \mathbf{n}_K d\sigma = 0, \text{ for all } X \in M_{h,K}, \\ &\sum_{\sigma=X|Y \in F_X \cap F_{h,K}^{int}} T_\sigma (u_X - u_Y) + \int_X \phi c / \Delta t u_X dx \\ &= \int_X (f + c\phi / \Delta t u_X^{n-1}) dx, \text{ for all } X \in M_{h,K}, \end{aligned} \right. \quad (12)$$

in which u_X^{n-1} stands for the pressure solution at the previous time step.

The previous time step solution on the right-hand side of the local source-problem makes the solution of this local source-problem time dependent. Moreover, if dynamic time-stepping strategy is adopted, the basis functions of the Local lambda problems need also to be updated at each time step for which Δt is modified.

As a validation test, a comparison between the fine scale finite volume method and FV-MHMM is given in Fig. 8. The test case is a centered wellbore with a constant rate of discharge $q_0 = -4.5 \cdot 10^{-5} \text{ m}^3 \cdot \text{s}^{-1}$ embedded in a square field of dimension $a = 3500 \text{ m}$. The fine-mesh discretization is 81×81 cells. The boundary conditions are considered to be homogeneous Neumann as stated in (11). The wellbore is active in the central cell. The homogeneous background permeability field is taken as equal to $K = 5 \cdot 10^{-13} \text{ m}^2$ throughout the whole domain. The compressibility is set at $3.9 \cdot 10^{-10} \text{ Pa}^{-1}$ with viscosity $\mu = 10^{-3} \text{ Pa} \cdot \text{s}$ and porosity $\phi = 0.25$.

We clearly note the accordance between the two solutions.

3.3 Two phase flow model

We generalized, in this section, the approach to incompressible immiscible two-phase flow. The saturations of the wetting and non-wetting phases are respectively referred to as S_w and S_n . We also introduce phases mobilities $\lambda_w(S_w)$ and $\lambda_n(S_n)$ as:

$$\lambda_w(S_w) = \frac{kr_w(S_w)}{\mu_w} \quad (13)$$

$$\lambda_n(S_w) = \frac{kr_n(S_w)}{\mu_n}$$

in which $kr_w(S_w)$ and $kr_n(S_w)$ denote the relative permeabilities respectively of the wetting and non-wetting phase. The dynamic viscosities of the wetting and non-wetting phases are introduced as μ_w and μ_n .

Let us introduce the generalized Darcy laws for the non-wetting phase, noted with subscript n , and for the wetting phase, noted with the subscript w , as :

$$\mathbf{v}_w = -K(\mathbf{x})\lambda_w(S_w)\nabla u, \quad (14)$$

$$\mathbf{v}_n = -K(\mathbf{x})\lambda_n(S_w)\nabla u.$$

The total Darcy velocity is defined as:

$$\mathbf{v} = -K(\mathbf{x})\lambda_t(S_w)\nabla u. \quad (15)$$

Here, the capillary pressure has been neglected, i.e., the wetting and non-wetting phase pressure are equal. From the

continuity equation of total flow and the mass balance in the wetting phase, a two-phase flow system is derived coupling an hyperbolic saturation equation with a parabolic pressure equation :

$$\begin{aligned} \nabla \cdot (-K(\mathbf{x})\lambda_t(S_w)\nabla u) &= f \quad \text{in } \Omega, \\ u &= u_g \quad \text{on } \partial\Omega_D, \\ \mathbf{v} \cdot \mathbf{n} &= q_0 \quad \text{on } \partial\Omega_N \\ \phi \frac{\partial S_w}{\partial t} + \nabla \cdot (f_w(S_w) \mathbf{v}) &= 0 \quad \text{in } \Omega, \\ \mathbf{v}_w \cdot \mathbf{n} &= q_{w,0} \quad \text{on } \partial\Omega_N. \end{aligned} \quad (16)$$

in which the fractional flow of the wetting phase $f_w(S_w) = \lambda_w(S_w)/\lambda_t(S_w)$ is defined.

Brooks and Corey models [4] for mobilities $\lambda_w(S_w)$, $\lambda_n(S_w)$ and $\lambda_t(S_w)$ are adopted here. They are written as:

$$\begin{aligned} \lambda_w(S_w) &= \frac{1}{\mu_w} \left(\frac{S_w - S_{n,res}}{1 - S_{w,c} - S_{n,res}} \right)^2, \\ \lambda_n(S_w) &= \frac{1}{\mu_n} \left(\frac{1 - S_w - S_{n,res}}{1 - S_{w,c} - S_{n,res}} \right)^2, \\ \lambda_t(S_w) &= \lambda_n(S_w) + \lambda_w(S_w). \end{aligned} \quad (17)$$

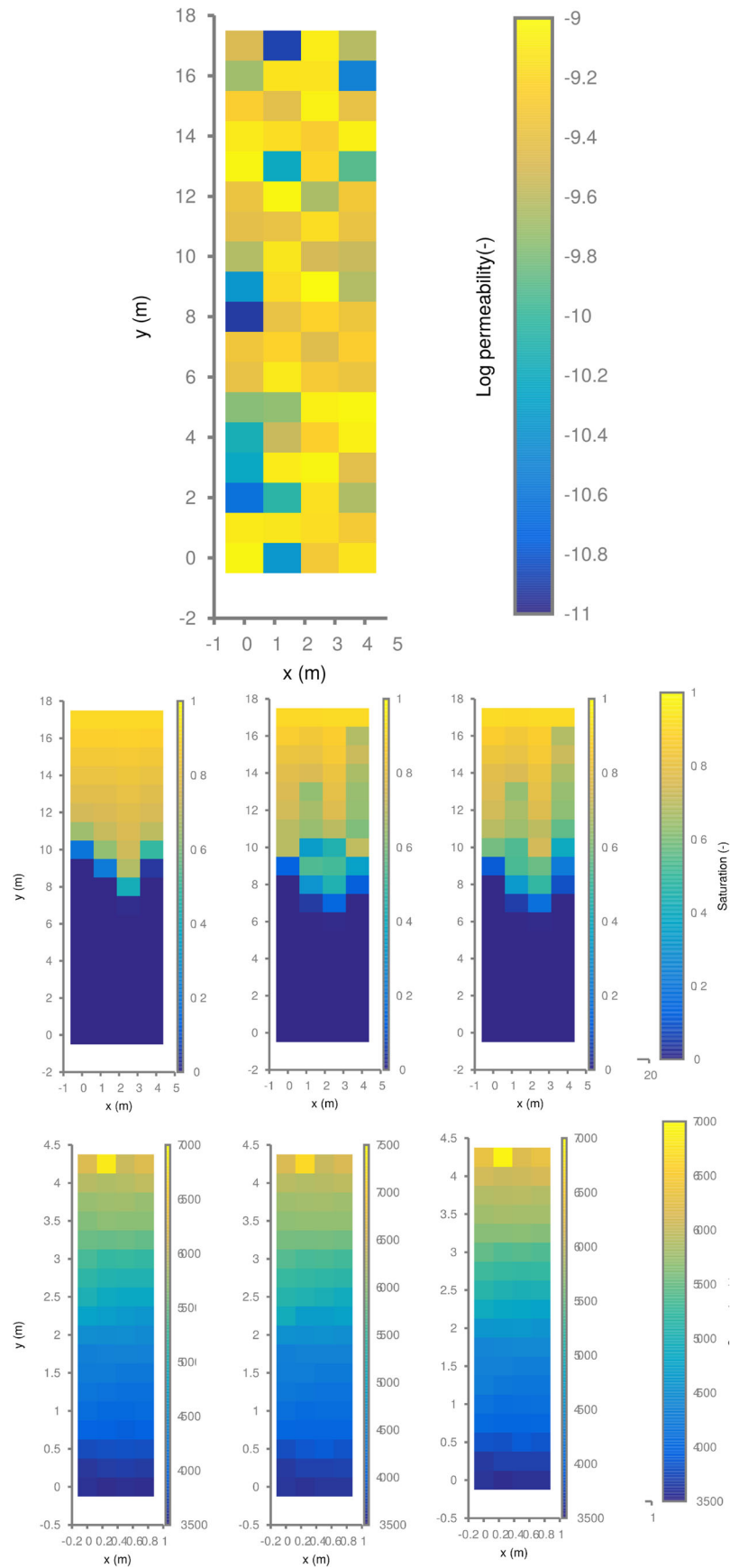
introducing the saturation parameters, $S_{n,res}$ and $S_{w,c}$ respectively residual non-wetting phase saturation and connate wetting phase saturation.

FV-MHMM algorithm is used to solve the pressure equation of the two-phase flow system (16), introducing transmissivity terms depending on the saturation $T_\sigma(S_w^{n+1})$. The hyperbolic saturation equation is solved using a first order upwind scheme. The two equations are coupled sequentially in the spirit of impes algorithm [22].

In order to validate two-phase flow implementation, we perform a Buckley Leverett test [5]. From this equation, front position and saturation are determined. The viscosity ratio is set to $\mu_w/\mu_n = 1$ and the injection rate is set at $q_0 = q_{w,0} = 2 \cdot 10^{-3} \text{ m}^3 \cdot \text{s}^{-1}$. Mobility parameters are defined as $S_{n,res} = S_{w,c} = 0$. The porosity is set to $\phi = 0.5$. On Fig. 9, the comparisons between front positions determined using the semi-analytical and from two phase flow FV-MHMM are reported. Here, a 6×1 coarse grid is used overlaying a 48×1 fine discretization. There is no loss of accuracy as shown on the right plot of Fig. 9, when compared to a finite volume simulation run on the fine grid discretization.

Next case involves a random permeability field through which a cross flow is performed. The porosity and Brooks and Corey parameters are kept at the previous values. Injection rate is set at $q_0 = 2 \cdot 10^{-4} \text{ m}^3 \cdot \text{s}^{-1}$. The injection of fluid with the same viscosity $\mu_w = \mu_n = 10^{-3} \text{ Pa} \cdot \text{s}$ is

Fig. 10 Detail of the comparison on a multiphase flow situation using FV-MHMM method at different orders and fine grid finite volume solution. Respectively, on the top logarithmic map of the permeability, on the bottom; from left to right, finite volume solution, two-phase *FV-MHMM* solution Δ_1 and Δ_2 for saturation and related pressure fields



studied. The overlaying coarse grid is kept at a 6×1 discretization level, while the fine grid is changed to a 48×4 discretization. A randomly generated permeability field is defined with $\mu(K) = 4.97 \cdot 10^{-10} \text{ m}^2$ with values ranging from $1.2 \cdot 10^{-11}$ to $9.97 \cdot 10^{-10} \text{ m}^2$. The reference is the fine grid solution obtained using OpenFOAM finite volume solver [14]. On Fig. 10, this solution is plotted on the left side. The saturation front is solely perturbed by local heterogeneities in permeability values. This reference is compared to Λ_1 , in the middle of Fig. 10, and Λ_2 , on the right side of Fig. 10, solution from two-phase FV-MHMM for $t = 34 \text{ s}$.

From Fig. 10, it can be noted again that refining Λ_l spaces switching from $l = 1$ to $l = 2$ allows us to capture more and more details of the solution. It provides us a new way of improving the solution without neither refining any meshes nor reducing time-step size.

4 Conclusion

In this paper, a new multiscale FV-MHMM method has been introduced for the resolution of the problem (1). This approach is based on a hybrid formulation of the pressure problem, where main unknowns are fluxes on the faces of a coarse mesh. Two kinds of local problems are involved: a local lambda problem (LLP) and a local source problem (LSP) in order to build the global problem. Each of these problems embeds local heterogeneity details. Considering flux basis functions as Lagrange multipliers, pressure continuity is weakly imposed on the coarse mesh. The mathematical formulation of this method has been presented and convergence has been tested on various test cases. Extensions of the FV-MHMM to slightly compressible cases and two-phase cases have been introduced.

FV-MHMM method is a promising method. Local problems are indeed entirely localized and could be run on different processors. Moreover, unlike classical finite volume methods, FV-MHMM offers possible degrees of refinement in the educated choice for the tests functions μ defined in spaces of polynomial functions Λ_l . Including a posteriori error estimators offers the possibility of local and adapted refinement of the Λ_l space.

Eventually, further works will focus on dealing with highly heterogeneous media and with cross-comparison with the main existing methods such as MsFv [16, 17], MsFEM [1, 15], GMsFEM [11], or numerical subgrid methods [2].

Acknowledgements This work was supported by STORENGY and ENGIE EPI. We would also like to thank Egermann Patrick and Ababou Rachid for their helpful comments and remarks on this work.

Appendix: A complexity analysis

[16] proposed a complexity analysis of their MsFv algorithm. Following their example, we will here remind their results and apply such an analysis on FV-MHMM to be able to compare the two approaches. The notations that will be used are introduced in Table 4.

Assuming that $t_1(n) \sim ct_m n^\alpha$ where t_m is the time spend for one multiplication, c and α constant depending on the solver. This complexity analysis neglects time spent in the reconstruction of the pressure and the fluxes leading to the following time by steps:

$$\begin{aligned} t_I &\approx N_n a_n c t_m \gamma^\alpha, \\ t_{II} &\approx N_v (a_v + 1) c t_m \gamma^\alpha \\ t_{III} &\approx c t_m N_v^\alpha. \end{aligned}$$

with the step *I* identified as construction of equivalent transmissivities for coarse scale fluxes, the step *II* as the construction of basis functions sets Φ on the primal grid and the step *III* as the solution on the coarse grid.

In the same manner, FV-MHMM can be analyzed as:

$$\begin{aligned} t_{LLP} &\approx 2d(l+1)N_v c t_m \gamma^\alpha, \\ t_{LSP} &\approx N_v c t_m \gamma^\alpha, \\ t_{GP} &\approx c t_m [N_v + (l+1)N_f]^\alpha. \end{aligned}$$

where d is the dimension number, l the order of the polynomial space used to approximate Λ_H as introduced in the paper. The step LLP is the local problem in terms of Lambda, the step LSP is the local problem in terms of source contribution and GP is the global problem also as introduced in the paper.

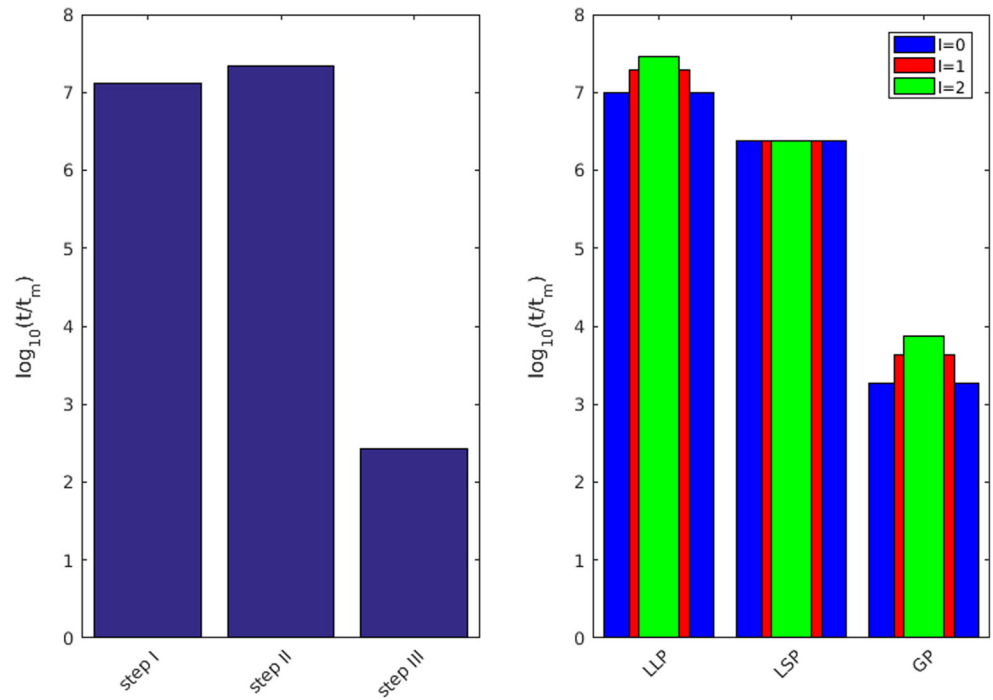
Table 4 Notations for complexity analysis

n_v	Number of volumes in the fine grid
N_v	Number of volumes in the coarse grid
N_n	Number of nodes in the coarse grid
N_f	Number of faces in the coarse grid
γ	Coarsening ratio $\sim n_v/N_v$
a_n	Number of adjacent coarse volume to a coarse node
a_v	Number of adjacent coarse volume to a coarse volume
$t_1(n)$	Time to solve a linear system with n unknowns

Table 5 Parameters of comparison

n_v	N_v	N_n	d	a_v	a_n	α	c
8100	9	12	2	8	4	1.5	10

Fig. 11 Time spent for the MsFv and the FV-MHMM in terms of operations



Considering an average number of coarse faces as $N_f \approx d(N_v^{1/d} + 1) \prod_{i=1}^{d-1} N_v^{1/d}$ with the parameters of Table 5, time used in term of t_m for each steps of both algorithms are represented on Fig. 11. It can be noticed that increasing polynomial order of approximation of Λ_H increases the computational cost for solving LLP and GP.

Increasing the order $l \in \{0, 1, 2\}$ of the polynomial space that approximated Λ_H , the speed up of FV-MHMM versus the MsFv method is respectively of 2.86, 1.59, and 1.10.

Moreover, the step I and step III are reported to be parallelizable for the MsFv method [16]. As for the FV-MHMM, all the local problems lambda (LLP) and local problems source (LSP) are independent from each other and therefore embarrassingly parallel. Moreover, the TPGA matrix for a selected coarse cell has to be generated only one time and can be used for solving both LLP and LSP associated with this coarse cell.

References

1. Aarnes, J.: On the use of a mixed multiscale finite element method for greater flexibility and increased speed or improved accuracy in reservoir simulation. *Multiscale Modeling & Simulation* (2004)
2. Arbogast, T.: Implementation of a locally conservative numerical subgrid upscaling scheme for two-phase darcy flow. *Computational Geosciences* (2002)
3. Brezzi, F., Douglas, J., Marini, L.D.: Two families of mixed finite elements for second order elliptic problems. *Numerische Mathematik* (1985)
4. Brooks, R., Corey, A.: Hydraulic properties of porous media and their relation to drainage design. *Transactions of the ASAE* (1964)
5. Buckley, S., Leverett, M., et al.: Mechanism of fluid displacement in sands. *Transactions of the AIME* (1942)
6. Carslaw, H., Jaeger, J. *Conduction of heat in solids*, 2nd edn. Clarendon Press, Oxford (1959)
7. Castelletto, N., Hajibeygi, H., Tchelepi, H.A.: Multiscale finite-element method for linear elastic geomechanics. *Journal of Computational Physics* (2016)
8. Chen, Z., Hou, T.: A mixed multiscale finite element method for elliptic problems with oscillating coefficients. *Mathematics of Computation* (2003)
9. Christie, M., Blunt, M., et al.: Tenth spe comparative solution project: A comparison of upscaling techniques. In: *SPE Reservoir Simulation Symposium*. Society of Petroleum Engineers (2001)
10. Dehkordi, M.M., Manzari, M.T.: Effects of using altered coarse grids on the implementation and computational cost of the multiscale finite volume method. *Advances in Water Resources* (2013)
11. Efendiev, Y., Galvis, J., Hou, T.Y.: Generalized multiscale finite element methods (gmsfem). *Journal of Computational Physics* (2013)
12. Harder, C., Paredes, D., Valentin, F.: A family of multiscale hybrid-mixed finite element methods for the darcy equation with rough coefficients. *Journal of Computational Physics* (2013)
13. Harder, C., Paredes, D., Valentin, F.: On a multiscale hybrid-mixed method for advective-reactive dominated problems with heterogeneous coefficients. *Multiscale Modeling & Simulation* (2015)
14. Horgue, P., Soulaire, C., Franc, J., Guibert, R., Debenest, G.: An open-source toolbox for multiphase flow in porous media. *Computer Physics Communications* (2015)
15. Hou, T., Wu, X.H.: A multiscale finite element method for elliptic problems in composite materials and porous media. *Journal of computational physics* (1997)

16. Jenny, P., Lee, S., Tchelepi, H.: Multi-scale finite-volume method for elliptic problems in subsurface flow simulation. *Journal of Computational Physics* (2003)
17. Jenny, P., Lee, S., Tchelepi, H.: Adaptive multiscale finite-volume method for multiphase flow and transport in porous media. *Multiscale Modeling & Simulation* (2005)
18. Lie, K.A.: An introduction to reservoir simulation using matlab. *SINTEF ICT* (2014)
19. Manea, A., Sewall, J., Tchelepi, H., et al.: Parallel multiscale linear solver for highly detailed reservoir models. In: *SPE Reservoir Simulation Symposium*. Society of Petroleum Engineers (2015)
20. Raviart, P.A., Thomas, J.: Primal hybrid finite element methods for 2nd order elliptic equations. *Mathematics of computation* (1977)
21. Renard, P., De Marsily, G.: Calculating equivalent permeability: a review. *Advances in water resources* (1997)
22. Sheldon, J., Cardwell, W., et al.: One-dimensional, incompressible, noncapillary. Two-phase fluid flow in a porous medium (1959)
23. Verdiere, S., Vignal, M.: Numerical and theoretical study of a dual mesh method using finite volume schemes for two phase flow problems in porous media. *Numerische Mathematik* (1998)
24. Wang, Y., Hajibeygi, H., Tchelepi, H.A.: Algebraic multiscale solver for flow in heterogeneous porous media. *Journal of Computational Physics* (2014)
25. Wood, B.: The role of scaling laws in upscaling. *Advances in Water Resources* (2009)